

Continuous Flow Synthesis of Cd_{1-x}Zn_xS and CdS/ZnS Core/Shell Semiconductor Nanoparticles by MicroJet Reactor Technology

Julia Hiemer and Klaus Stöwe*^[a]

From aqueous precursor solutions of metal salts and sodium sulfide using MicroJet Reactor (MJR) technology Cd_{1-x}Zn_xS and CdS/ZnS core/shell semiconductor nanoparticles were synthesized. The MJR approach represents an automated, continuous, flexible and scalable route for nanoparticle synthesis, providing a tight control over process parameters and thus simple size, shape and composition control. Since particle sizes below the excitonic Bohr radius were obtained by MJR, the nanoparticulate materials exhibit quantum confinement effects. By varying

the precursor ratio the band gap of Cd_{1-x}Zn_xS Quantum Dots (QDs) could be targeted from 3.1 to 3.6 eV. CdS/ZnS core/shell QDs were prepared by enclosing CdS particles from MJR with ZnS produced by thermal decomposition of a Zn-MPA complex. Adjustment of the shell thickness increased the photoluminescence intensity by 43%. Synthesis of ternary sulfides in the form of core/shell particles broadens the spectrum of materials accessible by MJR and demonstrates the extraordinary flexibility of the technology.

Introduction

Due to their size-dependent optical and electronic properties, nanoparticulate semiconductors with sizes below the excitonic Bohr radius have great potential for a variety of applications including photovoltaics,^[1] light-emitting diodes,^[2] displays,^[3] biological markers^[4] and photocatalysts for hydrogen production.^[5] Quantum confinement, which is expected for particle sizes below 10 nm, is responsible for the fundamental change in the physicochemical properties of the materials. By reducing dimensions, the electronic excitations shift to higher energy and are concentrated into just a few transitions.^[6] Depending on the particle size, the absorption and emission wavelengths of Quantum Dots (QDs) can be controlled from the ultraviolet (UV) to the infrared (IR) spectral range.^[7]

II–VI semiconductor nanoparticles, for example CdS and ZnS, exhibit a broad absorption as well as a narrow and tunable emission spectrum, intense luminescence in the visible light region and photostability.^[8,9] Owing to coordinatively unsaturated bonds and anisotropy, crystal defects in nanoparticles are often localized on the surface. Surface defects can lead to a significant broadening of photoluminescence (PL) emission and favor non-radiative recombination mechanisms. In particular, passivating of the surface of nanoparticles by epitaxial growth of a shell of a semiconductor material with a wider band gap,


for example in CdS/ZnS core/shell QDs, is resulting in an increase in PL intensity.^[10–14]

Since the exciton Bohr radius of CdS is exceptionally small at $a_B = 5.8$ nm,^[15] nanoparticle synthesis is a challenging task. A particularly promising approach is the continuous production of nanoparticles using microreactors or micromixers. Using continuous reactors can circumvent problems of the batch process concerning scale-up as a consequence of heat transfer, mixing dynamics and batch-to-batch reproducibility.^[16] The MicroJet Reactor (MJR),^[17] also known as an Impinging Jet Microreactor (IJMR), is a new design of a mixing device in principle similar to the Synthesechemie (Dr. Penth)^[18] or Ehrfeld microjet mixer as described by Dittert et al.^[19] The newly constructed MJR is completely dead volume free and allows the continuous preparation of nano-scale metal and metal chalcogenide particles by precipitation reactions from appropriate precursor solutions. Short mixing times in the μ s to ms range enable separation of crystallite nucleation and crystal growth. According to the model of LaMer and Dinigar,^[20] which describes particle formation by crystallization, concentration-limited particle growth leads to nanoparticles. Critical supersaturation is reached simultaneously in the MJR, resulting in a narrow particle size distribution (PSD).

Using appropriate surface modification, Penth^[21] showed the significant influence of the mixing velocity on particle size. Consequently, it is possible to control the PSD by selecting suitable reaction conditions in the MJR. An overview of materials already obtained by MJR technology is given in the following section.

Rüfer et al.^[22] obtained BaSO₄ nanoparticles with a hydrodynamic diameter $d_h = 60$ nm from precipitation of BaCl₂ and K₂SO₄ by controlling precursor concentration, flow velocity, dispersant and pressure. In comparison, particle sizes of approximately 300 nm were obtained in batch. A significant influence of the reaction conditions on particle size was not

[a] J. Hiemer, Prof. Dr. K. Stöwe
Institute of Chemistry, Faculty of Natural Sciences
Chemnitz University of Technology
Straße der Nationen 62, 09111 Chemnitz (Germany)
E-mail: klaus.stoeve@chemie.tu-chemnitz.de

 © 2022 The Authors. Published by Wiley-VCH GmbH. This is an open access article under the terms of the Creative Commons Attribution Non-Commercial NoDerivs License, which permits use and distribution in any medium, provided the original work is properly cited, the use is non-commercial and no modifications or adaptations are made.

discernible in the stirred-tank reactor (STR). Furthermore, MJR technology found application for the hydrolysis of titanium tetraethanolate in alcoholic solutions to produce TiO_2 nanoparticles with $d_h = 1\text{--}10$ nm.^[19] Characterization of the precipitates by powder X-ray diffraction showed a significant influence of the synthesis temperature on the crystalline phase composition of TiO_2 . By elevating the synthesis temperature from $T = 20$ to 210 °C, the anatase content increased from 34 to 75 %. Betke et al.^[23] employed the MJR for the synthesis of inorganic nanoparticles in aqueous media. Depending on the process parameters, uniform, spherical particles with $d_h = 44\text{--}102$ nm were obtained for ZnO, spherical particles with $d_h = 46\text{--}132$ nm for Fe_3O_4 and plate-shaped particles with a length of 100–500 nm for $\text{CaHPO}_4 \cdot \text{H}_2\text{O}$. The increase in temperature and flow rate caused a reduction in crystallite and particle size. Integrating co-precipitation in MJR, Clausing^[24] produced tantalum-doped tin oxides with high yields. A decrease of metal precursor concentration from $c_M = 0.025$ to 0.0125 mol L⁻¹ led to a reduction of $d_h = 1000$ to 140 nm. Desired doping levels $\chi_{\text{Ta}} = 5$ and 10% could be verified by means of X-ray fluorescence analysis. First efforts in the MJR synthesis of nanocrystalline metal chalcogenides were reported on by Hiemer et al.^[17] Precipitation of CdS was carried out from aqueous precursor solutions of $\text{Cd}(\text{NO}_3)_2$ and Na_2S . Electrostatic stabilization by an excess of sulfide or thiol ligands led to nanoparticles with $d_h = 2\text{--}6$ nm exhibiting quantum confinement effects.

The above-detailed literature review confirms the suitability of MJR technology for the continuous synthesis of inorganic materials, predominantly oxides, by precipitation reactions from aqueous precursor solutions. To broaden the spectrum of substances accessible by MJR, this work describes the syntheses and optical properties of composition-tuned $\text{Cd}_{1-x}\text{Zn}_x\text{S}$ and CdS/ZnS core/shell QDs. Correlations between composition and absorption and emission characteristics are highlighted.

Results and Discussion

A scheme for the synthesis of $\text{Cd}_{1-x}\text{Zn}_x\text{S}$ QDs (*Method 1*) and CdS/ZnS core/shell QDs (*Method 2*) is given in Figure 1. In *Method 1*, $\text{Cd}(\text{NO}_3)_2$, $\text{Zn}(\text{NO}_3)_2$ and the stabilizer 3-mercaptopropionic acid (MPA) were combined in one precursor solution. A second precursor solution containing the sulfide source Na_2S is used for the precipitation of $\text{Cd}_{1-x}\text{Zn}_x\text{S}$ QDs in MJR. CdS/ZnS core/shell QDs were obtained in a two-step synthesis. In MJR, CdS core particles are precipitated from $\text{Cd}(\text{NO}_3)_2$ and Na_2S . To the MPA-stabilized CdS QDs, a solution of $\text{Zn}(\text{NO}_3)_2$ and stabilizer is added. By heating the reaction mixture to $T_{\text{shell}} = 90$ °C, thermal decomposition of the Zn-MPA complex is induced to form a ZnS shell around the core particles.

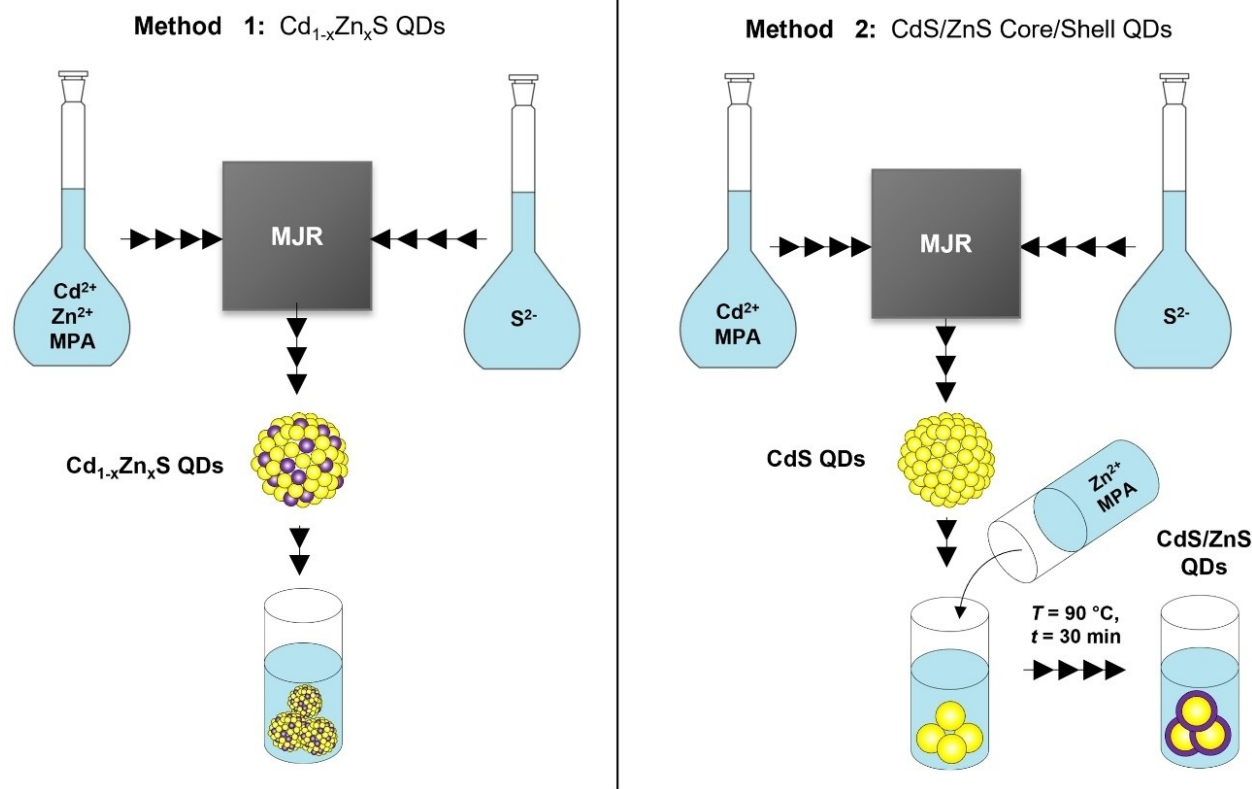


Figure 1. Strategy for the MicroJet Reactor (MJR) synthesis of $\text{Cd}_{1-x}\text{Zn}_x\text{S}$ QDs (*Method 1*) and CdS/ZnS core/shell QDs (*Method 2*) from $\text{Cd}(\text{NO}_3)_2$, $\text{Zn}(\text{NO}_3)_2$ and Na_2S solutions using 3-mercaptopropionic acid (MPA) for stabilization.

Cd_{1-x}Zn_xS Quantum Dots

Since CdS and ZnS crystallize isomorphously in sphalerite and wurtzite structure types, solid solutions of Cd_{1-x}Zn_xS QDs in the range $x=0-1$ can be formed. The experiments reported here focused on varying the composition and thus the optical properties resulting from the change in stoichiometry. For this purpose, the molar ratio $\text{Cd}^{2+}:\text{Zn}^{2+}$ was varied by means of the metal precursor concentration used in MJR synthesis.

For determination of the PSD of the suspensions from MJR synthesis, the hydrodynamic diameter obtained by means of dynamic light scattering (DLS) was analyzed (Figure 2). Similar hydrodynamic diameters were obtained for all compositions in a narrow size interval $1 < d_h(\text{Vol}) < 3$ nm. Since the exciton Bohr radius has been undercut for all compositions, the appearance of quantum confinement effects is highly probable. Verification

was carried out by investigating the optical properties of the nanomaterials.

The HOMO-LUMO gap energy E_g of semiconductors approximates the lowest optical excitation energy.^[25] To determine the band gap energy, linearization of the absorption spectra in Figure 3a using Tauc plots for direct semiconductors was carried out (Figure 3b). The intercept of the abscissa and a regression line of the linear region of maximum slope gives E_g as depicted in the inset. For binary CdS with $E_g(\text{bulk})=2.4$ eV,^[26] strong confinement is observed with $E_g=3.2\pm 0.02$ eV of the nanoparticulate material. Since all suspensions reveal the characteristic of $R/a_B < 1$, that is, are well within the strong confinement regime,^[27] the destabilization by the quantum energy is more significant than the exciton binding energy. According to the hypsochromic shift of the absorption edge of binary CdS with increasing amounts of Zn²⁺ in the precursor, the band gap is widened due to the larger band gap of ZnS

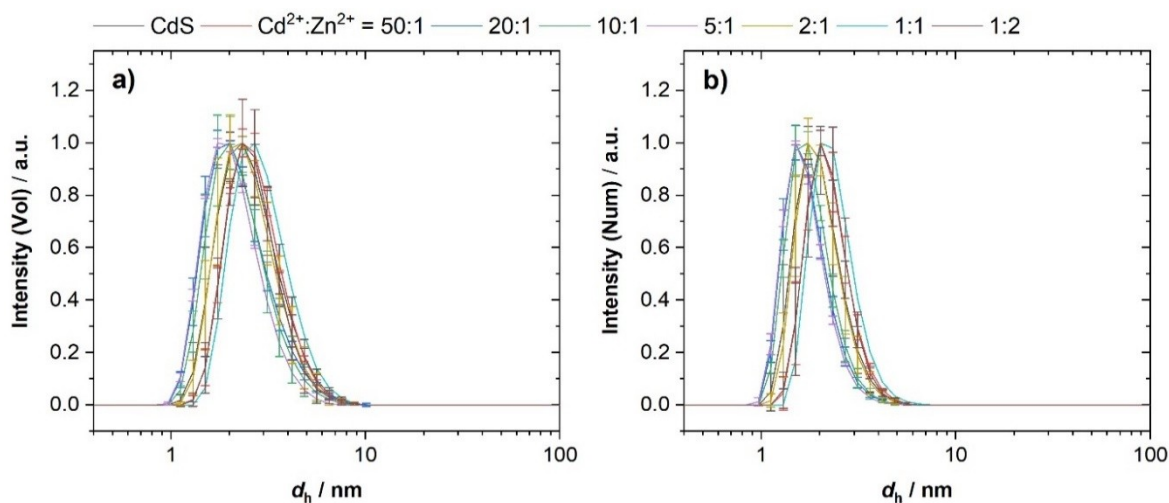


Figure 2. Volume (a) and number (b) distribution of hydrodynamic diameter d_h of Cd_{1-x}Zn_xS QDs analyzed by DLS. MJR synthesis from Cd(NO₃)₂, Zn(NO₃)₂ and Na₂S solutions using 3-mercaptopropionic acid (MPA) for stabilization. $\text{M}^{2+}:\text{MPA}:\text{S}^{2-}=2:5:1$, $c(\text{M}^{n+})=0.0125$ mol L⁻¹, $T=30$ °C.

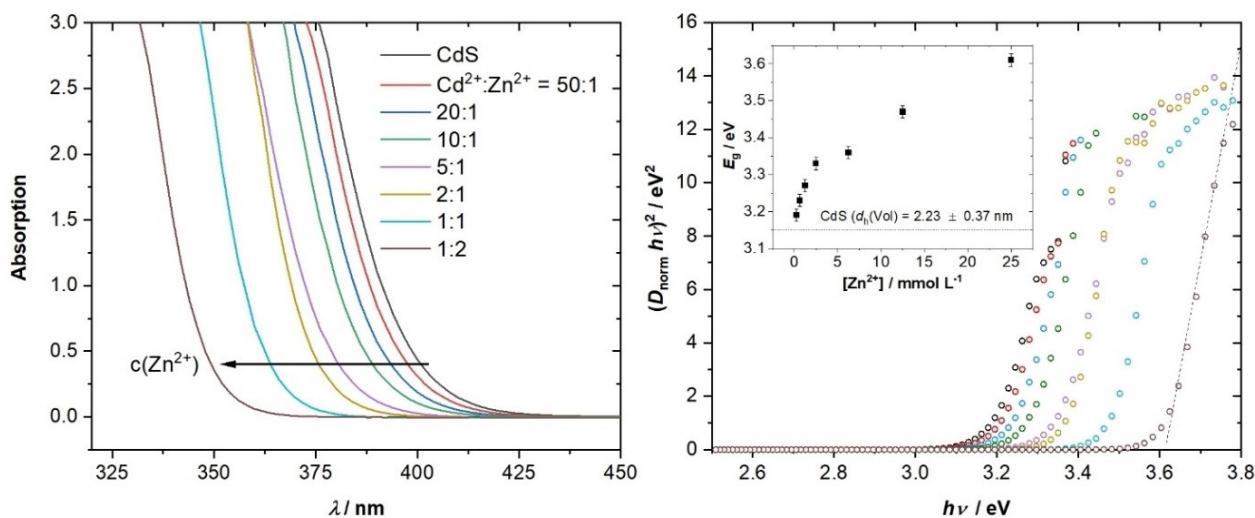


Figure 3. UV/Vis absorption spectra (a) and Tauc plots (b) of Cd_{1-x}Zn_xS QDs. MJR synthesis from Cd(NO₃)₂, Zn(NO₃)₂ and Na₂S solutions using 3-mercaptopropionic acid (MPA) for stabilization. $\text{M}^{2+}:\text{MPA}:\text{S}^{2-}=2:5:1$, $c(\text{M}^{n+})=0.0125$ mol L⁻¹, $T=30$ °C.

with $E_g(\text{bulk})=3.6\text{ eV}^{[28]}$ in comparison to CdS. At $c(\text{Zn}^{2+}) < 5\text{ mmol L}^{-1}$, the size of the band gap increases linearly. However, the curve flattens at higher Zn^{2+} contents. Given that the band gap energy of $\text{Cd}_{1-x}\text{Zn}_x\text{S}$ QDs is determined on the one hand by the composition and on the other hand by the size effect, a quantitative estimation of the influence of the two factors cannot be achieved based on the optical properties alone.

As shown in Figure 4, an elemental analysis by optical emission spectroscopy with inductively coupled plasma (ICP-OES) was carried out to determine the composition of the nanoparticles. Especially at low $c(\text{Zn}^{2+})$, the analytical results show lower molar ratios of $\text{Cd}^{2+}:\text{Zn}^{2+}$ than predetermined by the precursor composition. This effect decreases with increasing contents of Zn^{2+} , so that the excess of Zn^{2+} compared to the nominal content is almost balanced at $\text{Cd}^{2+}:\text{Zn}^{2+} \leq 2:1$. Consequently, the non-linearity in the trend of the band gap

energy can be attributed to a deviation of the nominal versus the targeted composition.

As can be seen in Figure 5a, $\text{Cd}_{1-x}\text{Zn}_x\text{S}$ QDs obtained by MJR syntheses exhibit a high degree of luminosity. In Figure 5b, the maximum of PL emission intensity $\lambda_{\text{em,max}}$ is shifted hypsochromically with increasing Zn^{2+} content as a result of the wider band gap of ZnS compared to CdS. A successive increase of the molar fraction of Zn^{2+} results in an optical shift from $\lambda_{\text{em,max}}=532\text{ nm}$ (2.33 eV) of binary CdS to 396 nm (3.13 eV) of $\text{Cd}_{0.33}\text{Zn}_{0.67}\text{S}$, covering the green to violet spectral range of visible light. The weak PL intensity of zinc-rich samples is a consequence of the too low excitation energy of the light source and emission of the QDs in the UV range.

For the verification of the particle size obtained by means of DLS, the sample $\text{Cd}_{1-x}\text{Zn}_x\text{S}$ with $x=0.1$ was further investigated by transmission electron microscopy (TEM), results of which are shown in Figure 6. The appearance of lattice fringes and the

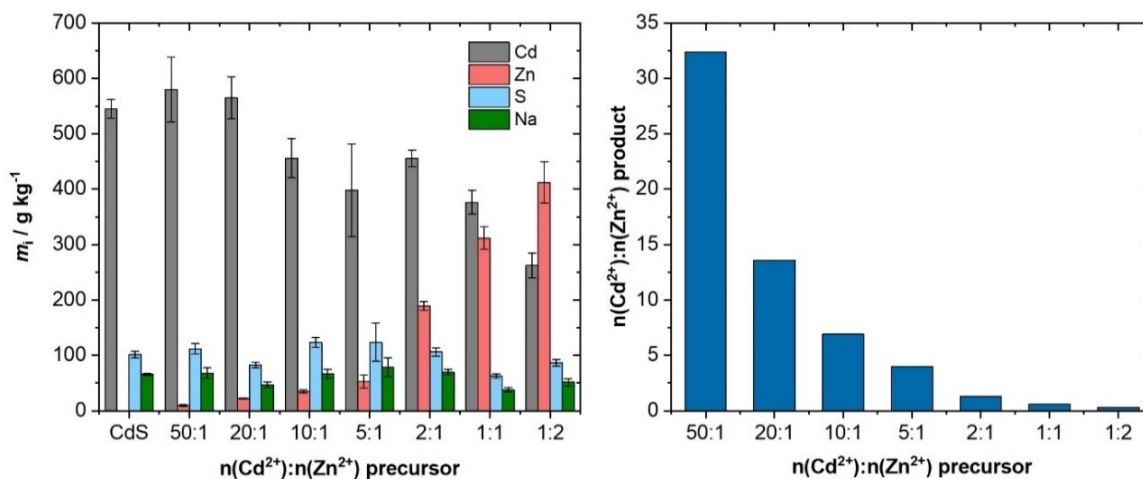


Figure 4. Elemental analysis of $\text{Cd}_{1-x}\text{Zn}_x\text{S}$ QDs by ICP-OES. MJR synthesis from $\text{Cd}(\text{NO}_3)_2$, $\text{Zn}(\text{NO}_3)_2$ and Na_2S solutions using 3-mercaptopropionic acid (MPA) for stabilization. $\text{M}^{2+}:\text{MPA}:\text{S}^{2-}=2:5:1$, $c(\text{M}^{n+})=0.0125\text{ mol L}^{-1}$, $T=30^\circ\text{C}$.

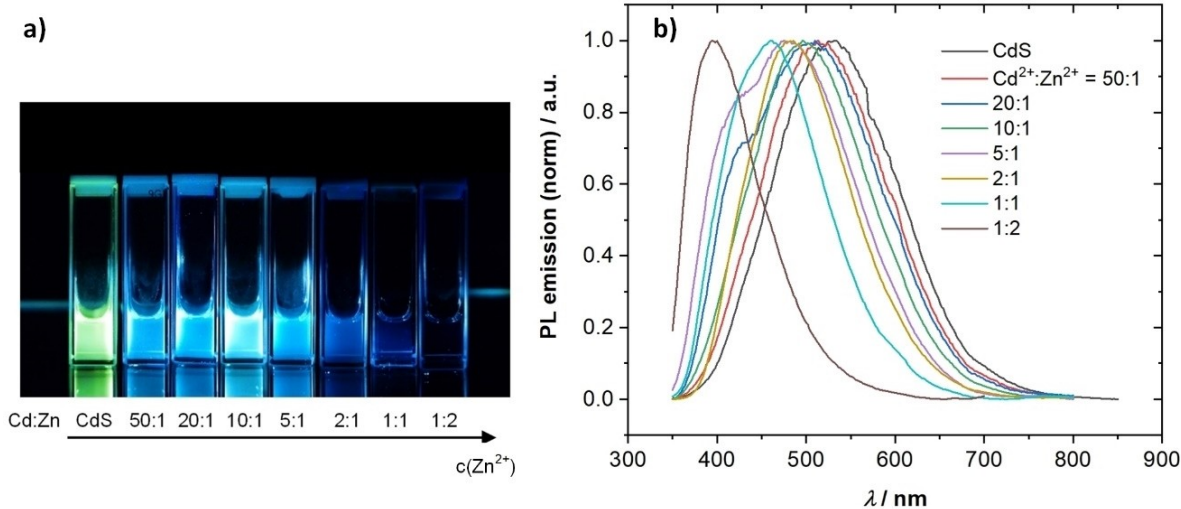


Figure 5. $\text{Cd}_{1-x}\text{Zn}_x\text{S}$ QDs under UV-light at $\lambda_{\text{exc}}=365\text{ nm}$ (a) and normalized PL-spectra at $\lambda_{\text{exc}}=300\text{ nm}$ (b). MJR synthesis from $\text{Cd}(\text{NO}_3)_2$, $\text{Zn}(\text{NO}_3)_2$ and Na_2S solution using 3-mercaptopropionic acid (MPA) for stabilization. $\text{M}^{2+}:\text{MPA}:\text{S}^{2-}=2:5:1$, $c(\text{M}^{n+})=0.0125\text{ mol L}^{-1}$, $T=30^\circ\text{C}$.

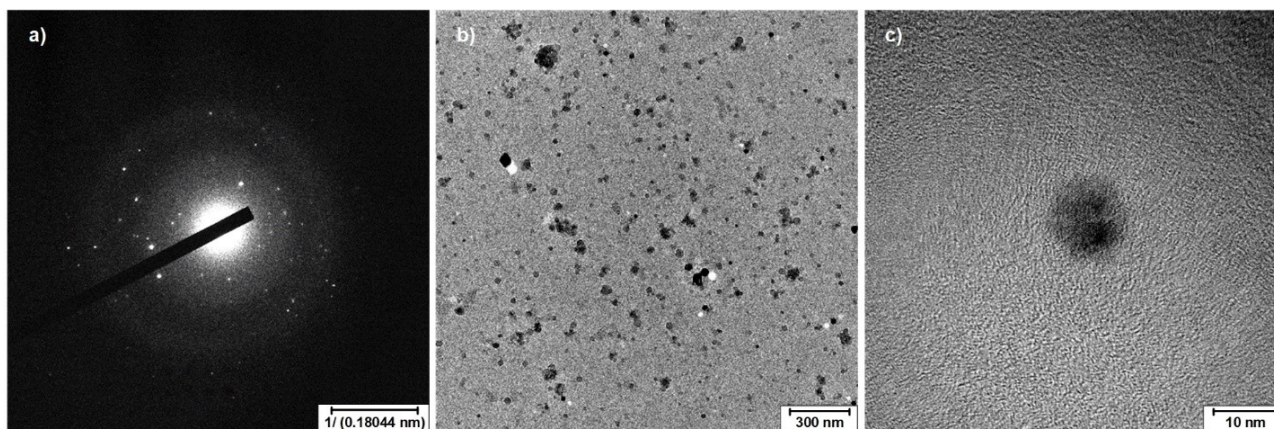


Figure 6. Diffraction pattern (a), overview (b) and single particle (c) TEM images of $\text{Cd}_{1-x}\text{Zn}_x\text{S}$ QDs. MJR synthesis from $\text{Cd}(\text{NO}_3)_2$, $\text{Zn}(\text{NO}_3)_2$ and Na_2S solutions using 3-mercaptopropionic acid (MPA) for stabilization. $\text{M}^{2+}:\text{MPA}:\text{S}^{2-} = 2:5:1$, $c(\text{M}^{n+}) = 0.0125 \text{ mol L}^{-1}$, $T = 30^\circ\text{C}$.

diffraction pattern confirm the crystallinity of the material. Unfortunately, high voltages of $U = 200 \text{ kV}$ caused agglomeration and additionally decomposition of particles. Few single particle images indicate particle diameters $d < 10 \text{ nm}$.

CdS/ZnS core/shell Quantum Dots

Various concentrations $c(\text{Zn}^{2+})$ were applied in the syntheses of CdS/ZnS core/shell QDs. It was investigated whether a change in the shell thickness possibly generated in this way has an influence on the material properties. Due to the bridging properties of Zn^{2+} and its function as a coagulant, preliminary experiments were conducted to define a concentration range in which stable nanoparticulate suspensions can be obtained. Since sedimentation occurs at molar metal ion ratios of $\text{Cd}^{2+}:\text{Zn}^{2+} < 2$ with $c(\text{Zn}^{2+}) > 6.25 \text{ mmol L}^{-1}$, lower quantities of Zn^{2+}

were used in the syntheses of core/shell QDs. The results of the DLS measurements are shown in Figure 7. After heating of the CdS suspension received directly from MJR synthesis with $d_{\text{max,Vol}} = 2.4 \pm 0.4 \text{ nm}$ to $T_{\text{shell}} = 90^\circ\text{C}$ for $t_{\text{shell}} = 30 \text{ min}$, an increase in hydrodynamic diameter to $5.4 \pm 0.4 \text{ nm}$ was observed. By adding Zn^{2+} , $d_{\text{max,Vol}}$ increased less during the temperature treatment. As the formation of ZnS shell is accompanied by a passivation of the nanoparticle surface and thus contributes to an increase in stability, this is a first hint towards the formation of core/shell particles.

The influence of the Zn^{2+} concentration on the absorption characteristics of the nanomaterials can be seen in Figure 8a. By tempering the pure CdS QDs suspensions, the absorption onset was bathochromically shifted by $\Delta\lambda \approx 100 \text{ nm}$. This is accompanied by a decrease of the band gap obtained from the Tauc plots in Figure 8b of $E_g = 3.15$ to $2.75 \pm 0.02 \text{ eV}$, corresponding to particle growth. An increase in $c(\text{Zn}^{2+})$ results in a

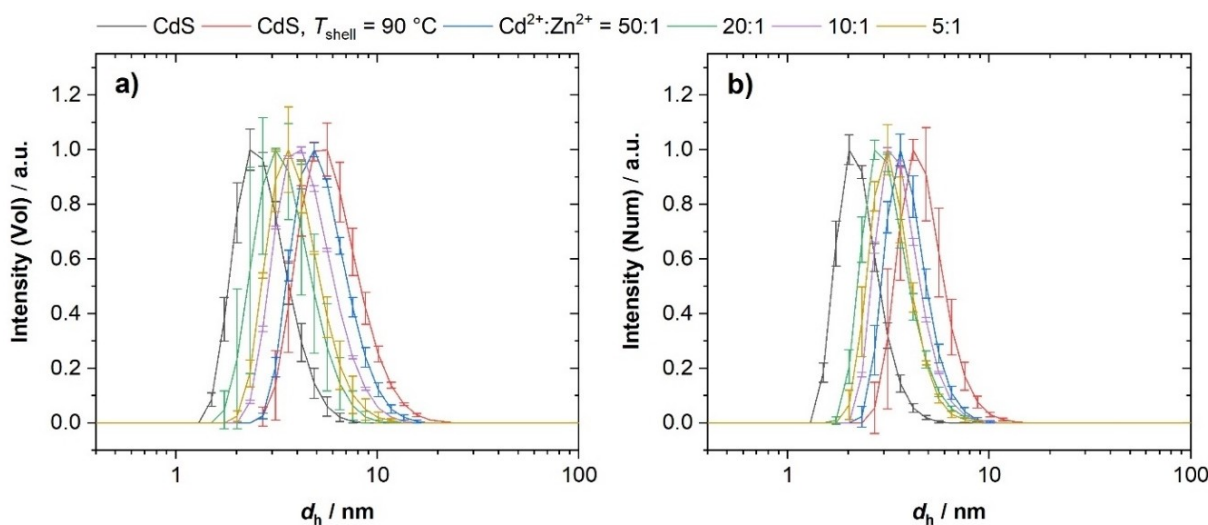


Figure 7. Volume (a) and number (b) distribution of hydrodynamic diameter d_h of CdS/ZnS core/shell QDs analyzed by DLS. MJR synthesis of CdS core from $\text{Cd}(\text{NO}_3)_2$ and Na_2S solutions using 3-mercaptopropionic acid (MPA) for stabilization. $\text{M}^{2+}:\text{MPA}:\text{S}^{2-} = 2:5:1$, $c(\text{M}^{n+}) = 0.0125 \text{ mol L}^{-1}$, $T = 30^\circ\text{C}$. Formation of ZnS shell by thermal decomposition of Zn-MPA complex at $T_{\text{shell}} = 90^\circ\text{C}$ for $t_{\text{shell}} = 30 \text{ min}$.

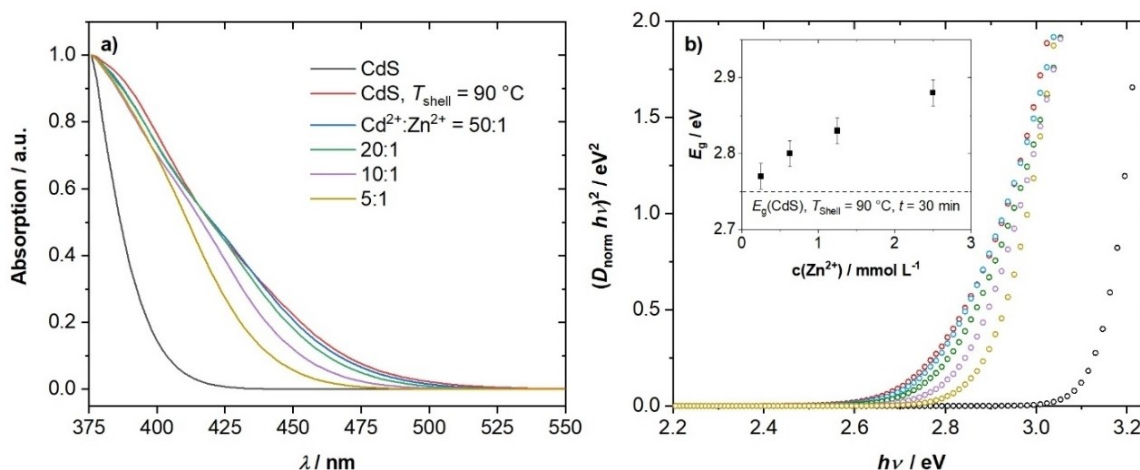


Figure 8. UV/Vis absorption spectra (a) and Tauc plots (b) of CdS/ZnS core/shell QDs. MJR synthesis of CdS core from $\text{Cd}(\text{NO}_3)_2$ and Na_2S solutions using 3-mercaptopropionic acid (MPA) for stabilization. $\text{M}^{2+}:\text{MPA}:\text{S}^{2-} = 2:5:1$, $c(\text{M}^{2+}) = 0.0125 \text{ mol L}^{-1}$, $T = 30^\circ\text{C}$. Formation of ZnS shell by thermal decomposition of Zn-MPA complex at $T_{\text{shell}} = 90^\circ\text{C}$ for $t_{\text{shell}} = 30 \text{ min}$.

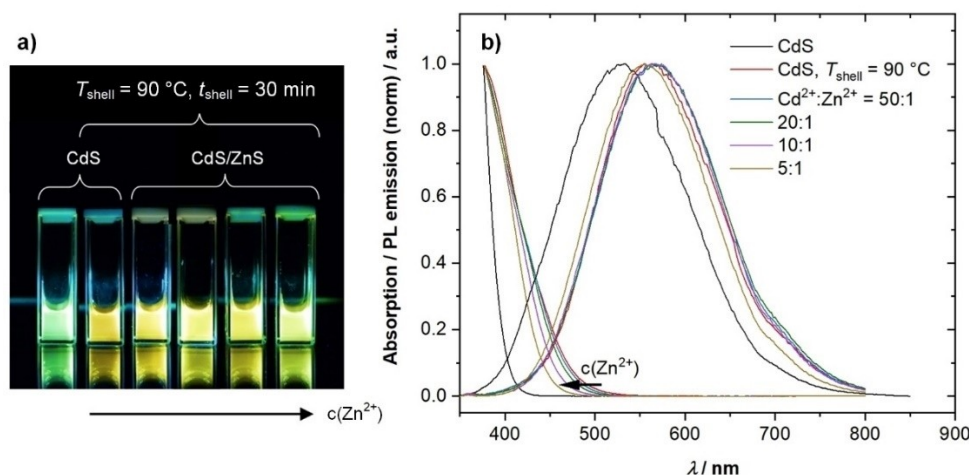


Figure 9. CdS/ZnS core/shell QDs under UV light at $\lambda_{\text{exc}} = 365 \text{ nm}$ (a) and normalized absorption/ PL spectra at $\lambda_{\text{exc}} = 340 \text{ nm}$ (b). MJR synthesis of CdS core from $\text{Cd}(\text{NO}_3)_2$ and Na_2S solutions using 3-mercaptopropionic acid (MPA) for stabilization. $\text{M}^{2+}:\text{MPA}:\text{S}^{2-} = 2:5:1$, $c(\text{M}^{2+}) = 0.0125 \text{ mol L}^{-1}$, $T = 30^\circ\text{C}$. Formation of ZnS shell by thermal decomposition of Zn-MPA complex at $T_{\text{shell}} = 90^\circ\text{C}$ for $t_{\text{shell}} = 30 \text{ min}$.

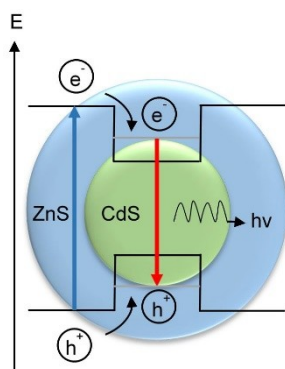


Figure 10. Simplified energy levels in core/shell QDs type I according to Ref. [31].

hypsochromic effect due to the larger band gap of ZnS compared to CdS.

Luminescence under UV light and normalized PL emission spectra of CdS/ZnS core/shell QDs are summarized in Figures 9a and 9b. As a result of particle growth, the maximum intensity of PL emission of the bare CdS QDs obtained directly from MJR synthesis shifts from $\lambda_{\text{em,max}} = 530$ to 565 nm due to temperature treatment. In contrast to the previous investigations, $\lambda_{\text{em,max}}$ of the core/shell QDs has nearly the same energy as bare CdS regardless of the precursor composition.

As shown in Figure 10, a spectral separation of absorption and emission occurs in different areas of the particles of type I core/shell materials.^[29,30] Fundamental absorption of photons of suitable energy produces an exciton in the shell relaxing to the

band edge states in the CdS core. Recombination of the exciton accompanied by emission of a photon takes place in the core. However, due to the small absorption cross section of nanoparticles, the absorption of the photon can proceed both in the shell and in the core.

Consequently, the absorption spectrum is characterized by core and shell material. PL emission wavelength is determined exclusively by the material properties of the core. Therefore, the shell thickness can be estimated from the absorption onset or the spectral width of the Stokes shift. As the concentration of Zn^{2+} increases, a hypsochromic shift of the absorption edge occurs due to increasing thickness of the ZnS shell. In particular, passivating of the surface of nanoparticles by epitaxial growth of a shell of a semiconductor material with a wider band gap

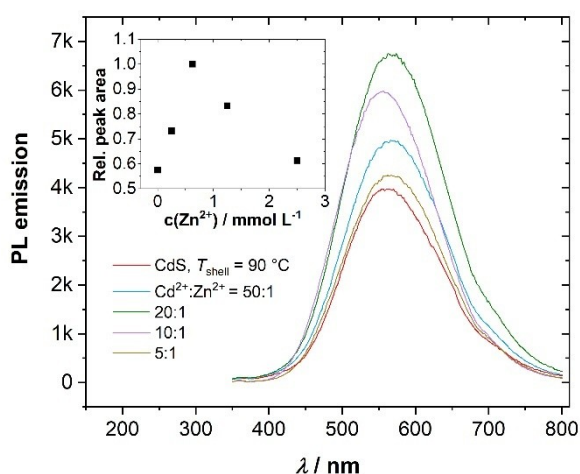


Figure 11. PL spectra and relative peak area (inlet) of CdS/ZnS core/shell QDs at $\lambda_{\text{exc}} = 340$ nm. MJR synthesis of CdS core from $\text{Cd}(\text{NO}_3)_2$ and Na_2S solutions using 3-mercaptopropionic acid (MPA) for stabilization. $M^{2+}:\text{MPA}:\text{S}^{2-} = 2:5:1$, $c(M^{n+}) = 0.0125 \text{ mol L}^{-1}$, $T = 30^\circ\text{C}$. Formation of ZnS shell by thermal decomposition of Zn-MPA complex at $T_{\text{shell}} = 90^\circ\text{C}$ for $t_{\text{shell}} = 30$ min.

leads to an increase in PL intensity.^[10–14] Several examples are given in the literature describing an increase of the PL intensity of CdS by applying a ZnS shell.^[14,32] Figure 11 depicts the unnormalized PL emission spectra of the CdS/ZnS core/shell QDs and the relative peak area obtained as a function of the molar Zn^{2+} concentration. Bare CdS particles exhibit the lowest PL intensity peak area. By adding the Zn-MPA complex up to $c(Zn^{2+}) = 6.25 \text{ mmol L}^{-1}$, the PL intensity could be increased by about 43%. A further increase of the Zn content leads to a decrease of the PL yield.

The results of the elemental analyses of the CdS/ZnS core/shell QDs performed by ICP-OES in Figure 12 show an increase in the Zn^{2+} content with increasing Zn^{2+} precursor concentration. Assuming all the Zn^{2+} ions in solution form a shell of defined diameter around the CdS core particles during the precipitation process, the shell thickness grows with increasing Zn^{2+} concentration in the reaction mixture. Confirmed by optical absorption investigations, in which an increasing Zn^{2+} precursor concentration led to a widening of E_g , the possibility to manipulate the shell thickness of the CdS/ZnS core/shell QDs by the metal salt concentration arises. Concentrations of sulfide and sodium ions, accumulating on the negatively charged particle surface, increase in consequence of the growing shell of ZnS and the expansion in total surface area.

TEM investigations were carried out for CdS/ZnS core/shell particles with $\text{Cd}^{2+}:\text{Zn}^{2+} = 5$, and results are displayed in Figure 13. Since the images show monodisperse, crystalline nanoparticles with $d_p < 5$ nm, the results of the DLS can be verified. The nanoparticles remained unchanged even under high acceleration voltage, confirming the stabilizing effect of the ZnS shell. The lattice fringe distance of $d = 0.33$ nm found most frequently in the images corresponds to lattice spacing of the plane (111) of the CdS phase Hawleyite and may be assigned to the CdS core material. Core/shell contrast cannot be visualized due to the resolution limit of the microscope and the low shell thickness of a few monolayers.

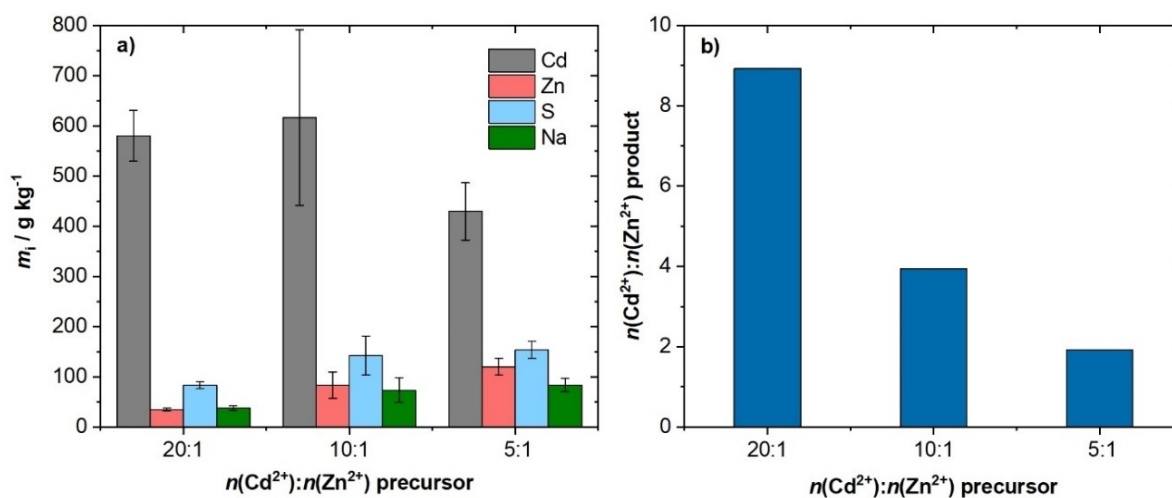


Figure 12. Elemental analysis by ICP-OES of CdS/ZnS core/shell QDs. MJR synthesis of CdS core from $\text{Cd}(\text{NO}_3)_2$ and Na_2S solutions using 3-mercaptopropionic acid (MPA) for stabilization. $M^{2+}:\text{MPA}:\text{S}^{2-} = 2:5:1$, $c(M^{n+}) = 0.0125 \text{ mol L}^{-1}$, $T = 30^\circ\text{C}$. Formation of ZnS shell by thermal decomposition of Zn-MPA complex at $T_{\text{shell}} = 90^\circ\text{C}$ for $t_{\text{shell}} = 30$ min.

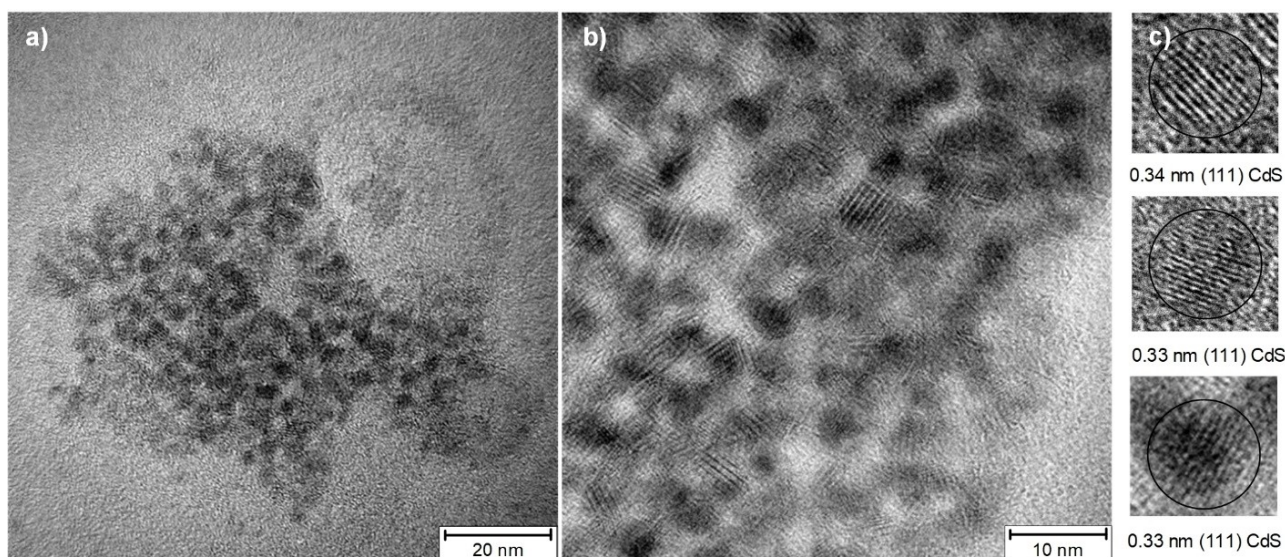


Figure 13. Overview (a,b) and single particle (c) TEM images of CdS/ZnS core/shell QDs. MJR synthesis of CdS core from $\text{Cd}(\text{NO}_3)_2$ and Na_2S solutions using 3-mercaptopropionic acid (MPA) for stabilization. $\text{M}^{2+}:\text{MPA}:\text{S}^{2-}=2:5:1$, $c(\text{M}^{n+})=0.0125\text{ mol L}^{-1}$, $T=30^\circ\text{C}$. Formation of ZnS shell by thermal decomposition of Zn-MPA complex at $T_{\text{shell}}=90^\circ\text{C}$ for $t_{\text{shell}}=30\text{ min}$.

Conclusions

By synthesis of $\text{Cd}_{1-x}\text{Zn}_x\text{S}$ mixed sulfide and CdS/ZnS core/shell Quantum Dots, the spectrum of materials accessible by continuous MJR technology has been extended. Due to the short mixing times compared to nucleation in the MicroJet Reactor, supersaturation is reached everywhere at once and all nuclei were formed synchronously from homogeneous solution, resulting in a narrow PSD. The particle growth could be stopped by consuming a precipitating component at the precursor concentrations used to obtain nanoparticulate suspensions within the scope of quantum confinement, as can be proved by means of DLS, TEM and optical investigations. Employing the ligand 3-mercaptopropionic acid, the nanoparticles showed exceptional stability.

The band gap and thus the optical properties of $\text{Cd}_{1-x}\text{Zn}_x\text{S}$ QDs could be targeted by means of the metal precursor ratio $\text{Cd}^{2+}:\text{Zn}^{2+}$. Absorption and emission bands are bathochromically shifted with increasing Zn^{2+} content due to the larger band gap of ZnS compared to CdS. In the investigated composition range of $x=0\text{--}0.67$, the band gap $E_g=3.1\text{--}3.6\pm 0.02\text{ eV}$ has been adjusted from the violet visible to the UV–A spectral range. Due to their high PL intensity, $\text{Cd}_{1-x}\text{Zn}_x\text{S}$ QDs are suitable for fluorescence applications. The PL emission wavelength ranges from $E_g(\lambda_{\text{em,max}})=2.3\text{ to }3.1\text{ eV}$, that is, from green to violet. Since the limiting precipitation component with a cation excess is the sulfide source, a variation of Na_2S concentration can be carried out in further experiments to selectively manipulate the nanoparticle size. In consequence, the spectral range tuned by the composition could be shifted and the spectral width preserved. Furthermore, the mixed sulfide QDs can be enclosed by a ZnS shell to increase stability and passivate surface defects for improved PL yield.

The investigation on the optical properties of CdS/ZnS core/shell QDs showed that the absorption is determined by both

the material of core and shell, while the emission wavelength depends entirely on size and composition of the core. Accordingly, variation of Zn^{2+} concentration to adjust the shell thickness had no influence on the PL emission wavelength with $\lambda\approx 565\text{ nm}$, but did influence the PL intensity. The highest value was obtained for a precursor ratio of $\text{Cd}^{2+}:\text{Zn}^{2+}=20:1$, with an increase in PL intensity of 43% compared to bare CdS. TEM proved the high crystallinity and stability of the core/shell particles. As described in *Method 2*, the core material was synthesized continuously by MJR, while the ZnS shell was deposited subsequently. Due to its modularity, the design of the MJR synthesis testing unit is suitable for expansion by a second MJR, for deposition of a ZnS shell on the previously precipitated CdS core particles. Hence, synthesis of complex structures such as core/shell particles would be possible in a continuous process.

The continuous MicroJet Reactor is superior to the batch reactor in terms of throughput. The following consideration will illustrate this: to produce $m=1\text{ g}$ CdS in the MJR in the form of quantum dots corresponding to a molar amount of $6.92\cdot 10^{-3}\text{ mol}$, with a sulfide concentration of $c(\text{S}^{2-})=6.25\cdot 10^{-4}\text{ mol L}^{-1}$ (electrostatically stabilized QDs), a volume of $V=11.092\text{ L}$ or a duration of $t(\text{MJR})=138.7\text{ min}$ is required assuming complete precipitation and a total volume flow of $\dot{V}=80\text{ mL min}^{-1}$. The assumption of a complete conversion was verified experimentally by UV/Vis spectrometry in the case of another QD system (Ag_2S). No further purification steps are necessary before usage of the QDs. In the present case, the reactor is at laboratory scale and can be scaled up accordingly for larger-scale syntheses. The possibility of scale-up is currently being investigated together with an industrial partner in a publicly funded project for the case of nanoscale fuel cell catalysis.

Experimental Section

Setup of the MJR

A detailed description of the MJR synthesis testing unit was provided by Hiemer et al.^[17] Figure 14 shows the simplified setup. Briefly, two High Performance Liquid Chromatography (HPLC) pumps transport the precursor solutions, typically aqueous solutions of metal salt(s) including stabilizer (P1) and sulfur source (P2), downstream from their reservoirs. Precursors are preheated in flow to the process temperature by passing a heat exchanger and directed through heated tubes to the MJR, in which the precipitation reaction takes place. The MJR itself consists of a cross-geometry tungsten carbide (WC) cube embedded in a stainless-steel housing enclosed by a heating sleeve. By forcing feeds with high pressure through narrow orifices of typically 100 μm , the flow rates are increased radically, and jets brought to collision under an angle of 180°. In contrast to the common T-mixer, the rapidly mixed product suspension is directly discharged by an orthogonal nitrogen flow. After passing a reaction path of variable length and temperature, cooling and gas-liquid separation, the nanoparticulate suspension is collected fractionally.

Nanomaterials Synthesis

Method 1: Cd_{1-x}Zn_xS Quantum Dots. Two separate stock solutions were prepared for metal precursor and precipitant. For the metal precursor solution, appropriate amounts of the metal salts cadmium(II) nitrate tetrahydrate ($\text{Cd}(\text{NO}_3)_2 \cdot 4\text{H}_2\text{O}$, 99.9%, Alfa Aesar) and zinc(II) nitrate hexahydrate ($\text{Zn}(\text{NO}_3)_2 \cdot 6\text{H}_2\text{O}$, 99.7% Alfa Aesar) were dissolved in ultrapure water. A total metal ion concentration $c(\text{M}^{n+}) = 12.5 \text{ mmol L}^{-1}$ was used. The stabilizer MPA was added with a molar ratio between metal salt:stabilizer:sulfide, $\text{M}^{n+}:\text{MPA}:\text{S}^{2-} = 2:5:1$. The turbid suspension was treated with 2 M NaOH until a clear solution was obtained. Typically, the pH for dissolution of the hydroxide varies from 7.5 to 8.5 and depends on the ratio of metal ions, $\text{Cd}^{2+}:\text{Zn}^{2+}$. According to $\text{M}^{n+}:\text{MPA}:\text{S}^{2-}$, an appropriate amount

sodium sulfide nonahydrate ($\text{Na}_2\text{S} \cdot 9\text{H}_2\text{O}$, 99%, Grüssing) was dissolved in ultrapure water to yield the precipitant solution.

For MJR synthesis, flow rates of $\dot{m} = 40 \text{ g min}^{-1}$ for each of the two precursors and an inert gas flow of $\dot{V} = 40 \text{ mL min}^{-1}$ were applied. All experiments were carried out at $T = 30^\circ\text{C}$. Pressure was maintained at $p = 20 \text{ bar}$ by a manual back-pressure regulator.

Method 2: CdS/ZnS core/shell Quantum Dots. MJR synthesis of the CdS core material was carried out analogously to *Method 1*, using exclusively $\text{Cd}(\text{NO}_3)_2$ as a metal precursor.

CdS/ZnS core/shell QDs were produced from CdS core suspensions obtained by MJR without further purification. A varying volume of aqueous $\text{Zn}(\text{NO}_3)_2$ solution containing the stabilizer MPA in an equimolar ratio was added to the core nanoparticles. For thermal decomposition of the Zn^{2+} -MPA-complex, the reaction mixture was heated to $T_{\text{shell}} = 90^\circ\text{C}$ and stirred for $t_{\text{shell}} = 30 \text{ min}$ at elevated temperature to form ZnS shell.

Characterization

Particle size distributions were determined using a Zetasizer Nano ZS from Malvern Instruments based on the principle of dynamic light scattering. The technology enables investigations of suspensions in the hydrodynamic diameter range $d_h = 0.6 \text{ nm}$ to $6 \mu\text{m}$. Laser light of $\lambda = 633 \text{ nm}$ and $P = 4 \text{ mW}$ was used as light source. The analyses were performed at an angle of 173° in backscattering arrangement (backscatter NIBS default). Depending on the concentration, suspensions were diluted in ultrapure water, filled into silica glass cuvettes (Hellma, EN 10204) and measured at $T = 20^\circ\text{C}$. Investigations were repeated in triplicate. The calculation of the PSD was carried out by the device according to Mie theory assuming spherical particles.

UV/Vis absorption spectra of nanoparticulate suspensions were recorded using a PowerWave XS microplate reader from BioTek Instruments Corp. in the wavelength range of $\lambda = 200\text{--}800 \text{ nm}$. Excitation was carried out with a xenon flash lamp. For microplate

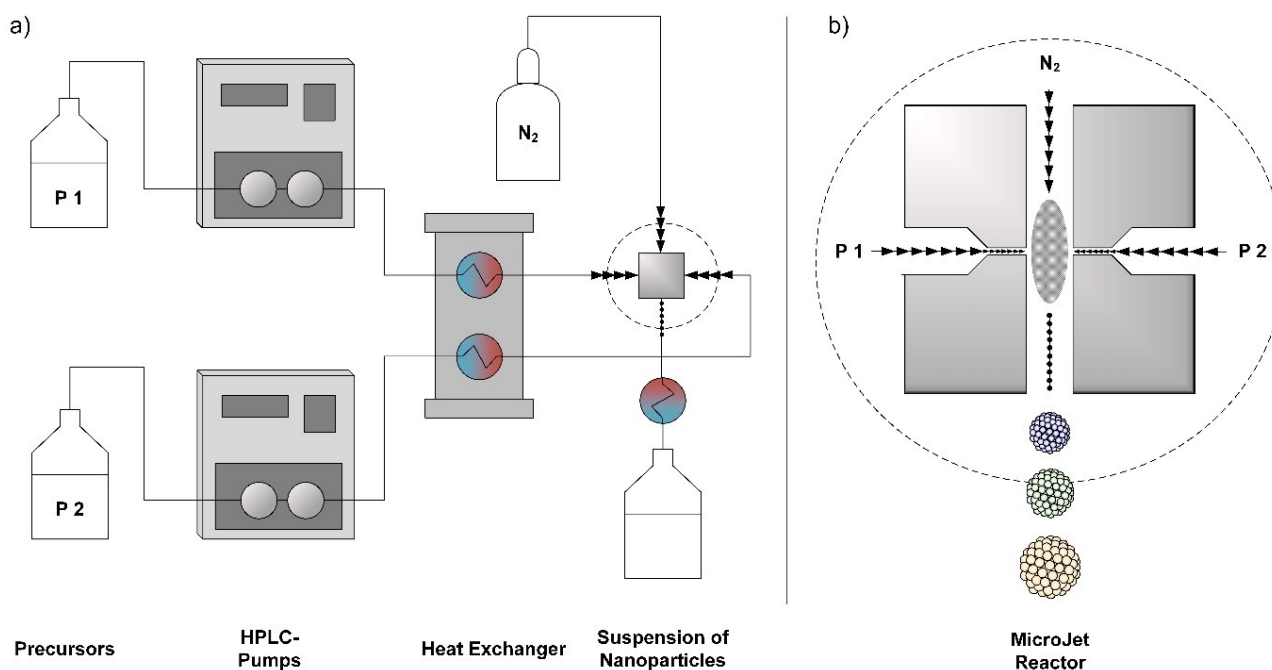


Figure 14. Simplified Setup of the MicroJet Reactor (MJR) synthesis testing unit (a) and cross section with collision zone (grey) of the MJR (b).

data acquisition and evaluation, the software Gen5 was used. Analysis was repeated in triplicate.

Investigations of photoluminescence properties were performed on a Cary Eclipse spectrometer from Agilent Corp. with emission wavelength 300 nm for Cd_{1-x}Zn_xS QDs and 340 nm for CdS/ZnS core/shell QDs. For acquisition, a volume V=0.1 mL of nanoparticulate suspension was filled in a silica glass cuvette and diluted in 2 mL of ultrapure water. Ten scans of each sample were recorded and averaged. Spectra were measured and evaluated using the Agilent WinFLR fluorescence software.

Transmission electron microscopy was performed using a PHILIPS CM 200 ST instrument at an acceleration voltage U=200 kV (point resolution 0.23 nm). Samples were prepared directly from the suspensions collected from MJR. A drop of the suspension was applied to a carbon-coated copper grid (200 mesh) purchased from Plano Corp. Prior to the investigation, samples were dried in high vacuum.

Optical emission spectroscopy with inductively coupled plasma for determination of the elemental composition of the metal sulfides was carried out on Vista Pro-RL spectrometer from Varian Corp. equipped with a CCD detector. Measurements were performed within t=5 min and with five repetitions. For investigations, 1000 ppm of the nanoparticulate powder obtained from aqueous suspension by nanofiltration was dissolved in 5 M HCl and treated for t=30 min in an ultrasonic bath. Elemental concentrations were obtained using ICP standard solutions of the elements cadmium, zinc, sulfur and sodium from Roth Corp.

Acknowledgements

The authors acknowledge the help of Prof. Dr. Andreas Schubert and Dr. Hennig Zeidler, Professorship Micromanufacturing Technology of the Chemnitz University of Technology (TUC) for their expertise and support in the MJR manufacturing process. Furthermore, the authors wish to thank Dr. Christopher Benndorf and Prof. Dr. Oliver Oeckler of the Materialwissenschaftliche Kristallographie of the Leipzig University for access and support with TEM facilities. We gratefully recognize the help of Daniel Beer and Prof. Dr. Carsten Deibel at TUC for the possibility to perform PL investigations.

Conflict of Interest

The authors declare no conflict of interest.

Data Availability Statement

The data that support the findings of this study are available from the corresponding author upon reasonable request.

Keywords: cadmium zinc sulfide · continuous flow synthesis · core/shell quantum dots · impinging jet microreactor · metal chalcogenide nanoparticles

- [1] S. Emin, S. P. Singh, L. Han, N. Satoh, A. Islam, *Sol. Energy* **2011**, *85*, 1264–1282.
- [2] S. Coe, W. K. Woo, M. Bawendi, V. Bulović, *Nature* **2002**, *420*, 800–803.
- [3] J. Mirzaei, M. Reznikov, T. Hegmann, *J. Mater. Chem.* **2012**, *22*, 22350–22365.
- [4] X. Gao, Y. Cui, R. M. Levenson, L. W. K. Chung, S. Nie, *Nat. Biotechnol.* **2004**, *22* (8), 969–976.
- [5] D. Prusty, L. Paramanik, K. Parida, *Energy Fuels* **2021**, *35*, 4670–4686.
- [6] A. P. Alivisatos, *Science* **1996**, *271*, 933–937.
- [7] S. V. Rempel', A. A. Razvodov, M. S. Nebogatikov, E. V. Shishkina, V. Y. Shur, A. A. Rempel', *Phys. Solid State* **2013**, *55*, 624–628.
- [8] V. Carrasco, V. Amarelle, S. L. Moraga, C. P. Quezada, R. E. González, R. Faccio, E. Fabiano, *Microb. Cell Fact.* **2021**, *41*.
- [9] S. Celebi, A. K. Erdamar, A. Sennaroglu, A. Kurt, H. Y. Acar, *J. Phys. Chem. B* **2007**, *111*, 12668–12675.
- [10] H. Weller, *Angew. Chem. Int. Ed.* **1993**, *32*, 41–53; *Angew. Chem.* **1993**, *105*, 43–55.
- [11] S. Wölper, Synthese und Oberflächenfunktionalisierung von III–V Halbleiternanopartikeln, PhD Thesis. Universität Hamburg (Germany), **2016**. <https://d-nb.info/1128310163/34>.
- [12] A. Raevskaya, V. Lesnyak, D. Haubold, V. Dzhagan, O. Stroyuk, N. Gaponik, D. R. T. Zahn, A. A. Eychmüller, *J. Phys. Chem. C* **2017**, *121*, 9032–9042.
- [13] F. Huang, Y. Lan, *Spectrosc. Lett.* **2015**, *48*, 159–162.
- [14] H. Kumar, P. B. Barman, R. R. Singh, *Phys. E: Low-Dimens. Syst. Nanostructures* **2015**, *67*, 168–177.
- [15] N. Razgoniaeva, P. Moroz, M. Yang, D. S. Budkina, H. Eckard, M. Augspurger, D. Khon, A. N. Tarnovsky, M. Zamkov, *J. Am. Chem. Soc.* **2017**, *139*, 7815–7822.
- [16] P. W. Dunne, C. L. Starkey, M. Gimeno-Fabra, E. H. Lester, *Nanoscale* **2014**, *6*, 2406–2418.
- [17] J. Hiemer, A. Clausing, T. Schwarz, K. Stöwe, *Chem. Eng. Technol.* **2019**, *42*, 2018–2027.
- [18] B. Penth, DE-10037301, **2002**.
- [19] B. Dittert, A. Gavrilović, S. Schwarz, P. Angerer, H. Steiner, R. Schöftner, *J. Eur. Ceram. Soc.* **2011**, *31*, 2475–2480.
- [20] R. H. Dinegar, V. K. LaMer, *J. Am. Chem. Soc.* **1950**, *72*, 4847–4854.
- [21] B. Penth, *Chem. Verfahren* **2004**, *6*, 94.
- [22] A. Rüfer, K. Rächle, F. Krahl, W. Reschetilowski, *Chem. Ing. Tech.* **2009**, *81*, 1949–1954.
- [23] A. Betke, G. Kickelbick, *Inorganics* **2014**, *2*, 1–15.
- [24] A. Clausing, Synthese und Charakterisierung Niob- und Tantal-dotierter Zinnoxide als potentielle Katalysatorträgermaterialien für Brennstoffzellen, PhD Thesis, Technische Universität Chemnitz (Germany), **2018**.
- [25] J. Frenzel, Structural, Electronic and Optical Properties of Cadmium Sulfide Nanoparticles. Thesis. Technische Universität Dresden **2007**.
- [26] S. M. Sze, K. K. Ng, *Physics of Semiconductor Devices*, 2. ed., Wiley Interscience, Hoboken, **1981**.
- [27] Y. J. Park, J. H. Oh, N. S. Han, H. C. Yoon, S. M. Park, Y. R. Do, J. K. Song, *J. Phys. Chem. C* **2014**, *118*, 25677–25683.
- [28] P. D'Amico, A. Calzolari, A. Ruini, A. Cattellani, *Nat. Sci. Reports* **2017**, *7*, 16805.
- [29] F. Purcell-Milton, Y. K. Gunko, *J. Mater. Chem.* **2012**, *22*, 16687–16697.
- [30] I. Coropceanu, M. G. Bawendi, *Nano Lett.* **2014**, *14*, 4097–4101.
- [31] D. U. Lee, D. H. Kim, D. H. Choi, S. W. Kim, H. S. Lee, K.-H. Yoo, T. W. Kim, *Opt. Express* **2016**, *24*, A350.
- [32] C. V. Reddy, J. Shim, M. Cho, *J. Phys. Chem. Solids* **2017**, *103*, 209–217.

Manuscript received: October 30, 2022